

Strong attenuation within the photonic band gaps of multiconnected networks

Zhen-Yu Wang^{1,*} and Xiangbo Yang^{1,2,†}

¹*MOE Key Laboratory of Laser Life Science & Institute of Laser Life Science, South China Normal University, Guangzhou 510631, China*

²*Laboratory of Photonic Information Technology, South China Normal University, Guangzhou 510631, China*

(Received 30 July 2007; published 5 December 2007)

We study the photonic band structures and the attenuation behavior of waves in configuration-periodic square networks where nearest-neighbor nodes are connected by more than one segment. It is shown that even though the period of the unit cell of a square network cannot be defined by the lengths of the segments and the nodes may not be arranged periodically in space, one can still use the Floquet-Bloch theorem in this network system if the theorem is modified. We find that the attenuation can be extremely large even though there is no absorption in the networks and its strength does not have a quasiparabolic profile as a function of wave frequency inside a gap. Large gaps and narrow passbands created by resonances and antiresonances are found.

DOI: [10.1103/PhysRevB.76.235104](https://doi.org/10.1103/PhysRevB.76.235104)

PACS number(s): 42.70.Qs, 41.20.Jb

I. INTRODUCTION

Dielectric structures with periodicities of their dielectric constant on a wavelength scale are capable of exhibiting a photonic band gap (PBG), where the propagation of electromagnetic (EM) waves is inhibited.^{1,2} In a PBG, the wave is Bragg scattered and the incident wave becomes an attenuate evanescent mode. This feature offers the possibility to confine and control the propagation of EM waves in PBG materials.^{3,4} One of the very important aspects of PBG systems is the wave attenuation at frequencies within the PBGs.⁵⁻⁷ PBG-based devices can have higher efficiency and be made smaller if the attenuation in the PBGs is larger.

A kind of PBG structure is a network system composed of one-dimensional (1D) waveguides.^{8,9} These systems are experimentally easily realizable, and the phase and amplitude can be measured anywhere inside the systems. It was found that introducing some loops in a network can produce band gaps and the loops will produce resonance at certain frequency range.⁸ However, to the best of our knowledge, the investigation of networks where all the adjacent nodes are connected by more than one segment has not been reported yet. In fact, connecting the adjacent nodes by more segments is equivalent to adding more loops to the system, and consequently, the possibility of producing resonance and antiresonance would be increased.

In this paper we study the band structures and the attenuation behavior of different EM modes inside the PBGs of square networks where nearest-neighbor nodes are connected by more than one segment in the same way. The configuration of this network is shown in Fig. 1, where the dashed lines between the adjacent nodes denote the same set of segments (shown on the left-hand side of Fig. 1). We call these networks square multiconnected networks (SMCNs).

It should be pointed out that only the configuration is necessarily periodic for the SMCNs. If the lengths of the segments connecting the nodes are different from each other, one cannot define the spatial period of the unit cell by these lengths. Additionally, the nodes may not be arranged in a square lattice. Consequently the conventional Floquet-Bloch theorem depending on spatial periodicity cannot be directly

applied. In this article we develop a dimensionless Floquet-Bloch theorem to study the present subject. This modified theorem can be used to investigate the networks of which only the configuration is periodic. In addition, by our method one can directly obtain the analytical results of the attenuation behavior of an EM wave in any direction inside the PBGs.

We find that due to resonances and antiresonances arising from the coherent waves of the segments between nearest-neighbor nodes, extremely narrow passbands near strong attenuation gaps are created and the attenuation inside the PBGs can be very large. In some circumstances, the strongest attenuation waves may appear near the band edges, rather than at the center of a band gap.

This paper is organized as follows: In Sec. II, we introduce the method for studying the mentioned network systems. An example of the use of this method is also presented. The band structures and the attenuation properties of SMCNs are investigated in Sec. III. Finally the conclusions are drawn in Sec. IV.

II. THEORY AND METHOD

The networks we study are formed by waveguide segments where only monomode propagation of EM waves

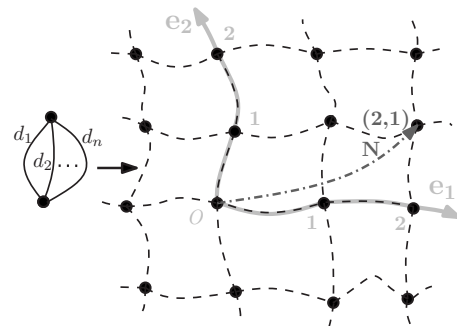


FIG. 1. Schematic diagram of a 2D square multiconnected network. The dashed lines denote n segments of various lengths connecting neighbor nodes. An $N=(2,1)$ is indicated by a dot-dashed arrow.

needs to be considered. The electromagnetic wave function with angular frequency ω in any segment between nodes i and j can be regarded as a linear combination of two opposite traveling plane waves:

$$\psi_{ij} = \alpha_{ij}e^{ikx} + \beta_{ij}e^{-ikx}, \quad (1)$$

with $k = \omega/c$, where c is the speed of the EM wave in the segment. For networks consisting of coaxial cables, the function ψ_{ij} represents the voltage wave.⁸ The wave function is continuous at the nodes of a network:

$$\begin{aligned} \psi_{ij}|_{x=0} &= \psi_i, \\ \psi_{ij}|_{x=l_{ij}} &= \psi_j, \end{aligned} \quad (2)$$

where ψ_i and ψ_j are the wave functions at nodes i and j , respectively, and l_{ij} is the length of the segment between nodes i and j . At any node i , the energy flux conservation gives

$$\sum_j \frac{1}{\mu\omega} \psi_{ij} \left. \frac{\partial \psi_{ij}}{\partial x} A_{ij} \right|_{x=0} = 0, \quad (3)$$

where the summation is over all segments linked directly to node i . When the cross-sectional area A_{ij} for each segment is the same, the boundary conditions, Eqs. (2) and (3), yield

$$\sum_j \left. \frac{\partial \psi_{ij}}{\partial x} \right|_{x=0} = 0. \quad (4)$$

By means of the continuity condition, Eq. (2), one can rewrite Eq. (1) as follows:

$$\psi_{ij} = \frac{\sin[k(l_{ij}-x)]}{\sin kl_{ij}} \psi_i + \frac{\sin kx}{\sin kl_{ij}} \psi_j. \quad (5)$$

Substituting Eq. (5) into Eq. (4), we obtain the network equation¹⁰

$$-\psi_i \sum_j \cot kl_{ij} + \sum_j \psi_j \csc kl_{ij} = 0, \quad (6)$$

where \cot and \csc are the cotangent and cosecant functions, respectively. Equation (6) is valid when the cross-sectional diameter for each waveguide segment is much smaller than the length and thus only monomode propagation of electromagnetic waves needs to be considered in these waveguide segments. For systems with dissipation, the wave vector k in Eq. (6) is a complex number,⁸ but we only consider ideal lossless waveguides in this paper, where k is always real.

Generally, for the network systems where nearest-neighbor nodes are connected by one or some segments of the same length, one can obtain the band structures by solving a set of coupled equations (6) with the use of the Floquet-Bloch theorem.¹¹ However, as we have mentioned previously, the Floquet-Bloch theorem cannot be directly applied to networks where the spatial period is not defined.

We notice that the conventional Floquet-Bloch theorem states that, for example, in the case of 1D when we make a lattice translation of a unit cell, the Bloch function is multiplied by a phase factor $\exp(iK'a)$, where K' is the Bloch wave vector and a the lattice constant. Actually, this phase

factor can be denoted more generally by $\exp(iK)$, where K is dimensionless. This phase change for the Bloch function should be more universal and should still hold in network systems in which only the configuration is periodic. Hence, we consider that under a discrete configuration translation for a network system the Bloch function is multiplied by a factor $\exp(iK)$, even though the spatial period is not defined. The K mentioned above can be regarded as a dimensionless Bloch wave vector and does not depend on the lattice constant.

More explicitly, for a configuration-periodic network, there is the following relation for the Bloch function when a discrete configuration translation \mathbf{T} is made:

$$\psi_{\mathbf{K}}(\mathbf{N} + \mathbf{T}) = \psi_{\mathbf{K}}(\mathbf{N})e^{i\mathbf{K}\cdot\mathbf{T}}, \quad (7)$$

where \mathbf{T} , \mathbf{N} , and \mathbf{K} are all dimensionless and their values depend on the configuration of the network.

In a 2D network, $\mathbf{T}=(T_1, T_2)$, $\mathbf{N}=(N_1, N_2)$, and $\mathbf{K}=(K_1, K_2)$ all have two components with respect to the configuration ‘‘directions’’ \mathbf{e}_1 and \mathbf{e}_2 . T_1 and T_2 being integers are, respectively, the numbers of discrete configuration translations along \mathbf{e}_1 and \mathbf{e}_2 . The location of a node is indicated by a pair of node indices N_1 and N_2 . An $\mathbf{N}=(2, 1)$ is shown in Fig. 1 as an example. The elements of the dimensionless Bloch wave vector \mathbf{K} —namely, K_1 and K_2 —are the phase changes. If a system has a spatial period, for example, with a 2D translation vector $\mathbf{a}=(a_1, a_2)$, then $(\frac{K_1}{a_1}, \frac{K_2}{a_2})$ represents the conventional Bloch wave vector.

Then the Floquet-Bloch theorem has been modified to a dimensionless one. One can then obtain the band structure or dispersion relation $\omega(\mathbf{K})$ for any periodic network by using Eqs. (6) and (7).

When \mathbf{K} is real, the wave is a propagation mode and can travel through the network without attenuation, whereas in the PBG wave is an evanescent mode with complex \mathbf{K} .¹² The imaginary part of \mathbf{K} , $\text{Im } \mathbf{K}$, describes quantitatively the attenuation of the wave amplitude as it propagates through the network. In this paper $\text{Im } \mathbf{K}$ denotes only the positive solution of Eq. (7), since if \mathbf{K} is a solution, so is $-\mathbf{K}$ and a positive $\text{Im } \mathbf{K}$ corresponds to the amplitude attenuation constant¹³ (dimensionless).

The attenuation within a gap is due to the destructive interference of scattered waves. In a PBG the incident wave is Bragg reflected and the wave intensity decays away from the boundary with a certain decrement. If the nodes of a 1D network are arranged periodically in space, this decrement can also be described by the Bragg attenuation length (localization length) (Refs. 14 and 15) L_B . With this condition, the Bragg attenuation length is given by $L_B = a/\text{Im } K$, where a is the spatial period. Hence, a larger $\text{Im } K$ will cause a shorter Bragg attenuation length L_B .

We use the following example to illustrate the use of Eqs. (6) and (7) and to evaluate our suggestion. Consider a quasi-1D periodic serial loop network shown in Fig. 2, which has been investigated in Ref. 16 by a method based on interface response theory.¹⁷ The lengths of the segments in a periodic unit and some node indices are indicated in the figure.

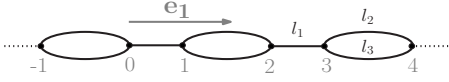


FIG. 2. Schematic diagram of a quasi-1D periodic serial loop network.

From Eq. (6), we obtain the relation of the wave functions for nodes at $N=0, 2$, and 4:

$$-\left(\sum_{j=1}^3 \cot kl_j\right)^2 \psi_K(2) + [\csc^2 kl_1 + (\csc kl_2 + \csc kl_3)^2] \psi_K(2) + \csc kl_1 (\csc kl_2 + \csc kl_3) [\psi_K(0) + \psi_K(4)] = 0. \quad (8)$$

The discrete configuration translation of this structure exists. Hence, from Eq. (7) the wave functions at nodes 0 and 4 are related to that at node 2 in the following equations:

$$\begin{aligned} \psi_K(4) &= \exp(iK) \psi_K(2), \\ \psi_K(0) &= \exp(-iK) \psi_K(2). \end{aligned} \quad (9)$$

The dispersion relation of this network is then obtained by substituting Eq. (9) into Eq. (8) and from the condition of existence of nontrivial solutions,

$$\begin{aligned} \cos K &= \frac{1}{2 \sin\left(\frac{kL}{2}\right) \cos\left(\frac{k\delta L}{2}\right)} \left[\cos kl_1 \sin kL \right. \\ &\quad \left. + \sin kl_1 \left(\frac{5}{4} \cos kL - \frac{1}{4} \cos k\delta L - 1 \right) \right], \end{aligned} \quad (10)$$

with $L=l_2+l_3$ and $\delta L=l_2-l_3$, which is exactly the result obtained by a different approach reported in Ref. 16. It shows that our approach is convenient and powerful.

III. BAND STRUCTURES AND ATTENUATION OF SQUARE MULTICONNECTED NETWORKS

Consider a 2D square multiconnected network where nearest-neighbor nodes are connected by n segments (Fig. 1). We first deduce the dispersion relation of this network. Equation (6) for the node at $\mathbf{N}=(0,0)$ reads

$$\begin{aligned} -4\psi_{\mathbf{K}}(0,0) \sum_{j=1}^n \cot kd_j + \sum_{j=1}^n \csc kd_j [\psi_{\mathbf{K}}(-1,0) + \psi_{\mathbf{K}}(1,0) \\ + \psi_{\mathbf{K}}(0,-1) + \psi_{\mathbf{K}}(0,1)] = 0, \end{aligned} \quad (11)$$

where d_j is the length of the j th segment connecting the same pair of adjacent nodes, and Eq. (7) gives

$$\begin{aligned} \psi_{\mathbf{K}}(1,0) &= \exp(iK_1) \psi_{\mathbf{K}}(0,0), \\ \psi_{\mathbf{K}}(-1,0) &= \exp(-iK_1) \psi_{\mathbf{K}}(0,0), \\ \psi_{\mathbf{K}}(0,1) &= \exp(iK_2) \psi_{\mathbf{K}}(0,0), \end{aligned}$$

$$\psi_{\mathbf{K}}(0,-1) = \exp(-iK_2) \psi_{\mathbf{K}}(0,0). \quad (12)$$

The dimensionless Bloch wave vector $\mathbf{K}=(K_1, K_2)$ has two components corresponding to the phase changes along \mathbf{e}_1 and \mathbf{e}_2 , respectively.

By substituting Eq. (12) into Eq. (11) and from the condition of existence of nontrivial solutions, the dispersion relation of this network is obtained:

$$\cos K_1 + \cos K_2 = f(k) = f\left(\frac{\omega}{c}\right), \quad (13)$$

where

$$f(k) = 2 \left(\sum_{j=1}^n \cot kd_j \right) / \left(\sum_{j=1}^n \csc kd_j \right). \quad (14)$$

Similarly, the dispersion relation of a square multiconnected network in η dimensions can be deduced,

$$\sum_{i=1}^{\eta} \cos K_i = \eta \left(\sum_{j=1}^n \cot kd_j \right) / \left(\sum_{j=1}^n \csc kd_j \right). \quad (15)$$

For simplicity, we only discuss the results for the 2D networks, since other dimensional ones will have similar properties. We first consider the SMCNs that every pair of adjacent nodes is connected by $n=2$ segments, and their band structures are shown in Fig. 3 for different ratios of d_2/d_1 . The symmetry points Γ , \mathbf{X} , and \mathbf{M} correspond to $\mathbf{K}=(0,0)$, $(\pi,0)$, and (π,π) , respectively.

When $d_2=d_1$, Eq. (14) reduces to a very simple form, i.e., $f(k)=2 \cos kd_1$. Therefore, for any frequency Eq. (13) always has real solutions for \mathbf{K} . Thus no gap exists in the SMCNs with this condition, which can be seen in Fig. 3(b). Actually, a SMCN which satisfies this condition is equal to a square network where nearest-neighbor nodes are connected by one segment, since the only difference between these two networks is the magnitude of waves traveling from one node to the other node, which does not break the scattering patterns.

When d_2 is slightly different from d_1 , the symmetry of the two propagation channels is broken and a small resonance occurs, which results in a narrow gap [Fig. 3(c)]. The segments with different lengths between every pair of adjacent nodes form an asymmetric loop similar to an acoustic loop filter device.¹⁸ The band structure of a SMCN with $d_2=2d_1$ is plotted in Fig. 3(a), where a large gap with a width of $\pi c/d_1$ can be seen. The gap to midgap ratio for this large gap is as large as 100%. This gap is mainly due to the destructive interference, since the path difference $\Delta d=d_2-d_1$ between the long and short segments differs by one-half wavelength at the frequency $\omega_c=\pi c/d_1$, which also is the midgap frequency of the gap. It is easy to see from Eq. (6) that the band structure is periodic in ω with a period $2\pi c/d_1$. Hence the stop bands and the passbands are periodically separated and of the same width $\Delta\omega=\omega_c$.

It is interesting that a very narrow passband can be created at about the center of the large band gap when d_2 is slightly different from $2d_1$, as can be seen in Fig. 3(d), where $d_2=1.98d_1$ and a narrow passband appears around $1.005\pi c/d_1$ with a width of approximately $0.01\pi c/d_1$. The

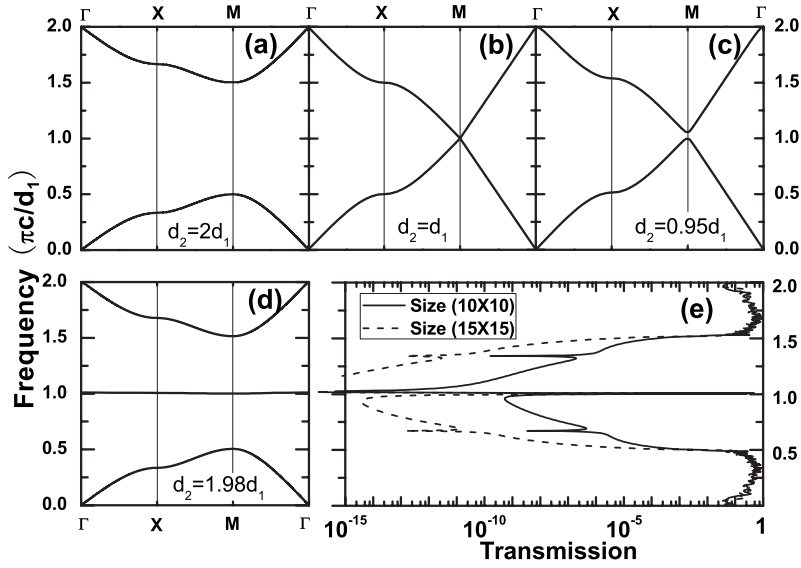


FIG. 3. (a)–(d) Band structures of the SMCNs with $n=2$ for different relative lengths of segments. (e) Total transmissions of the SMCNs with a size of 10×10 nodes (solid curve) and 15×15 nodes (dashed curve). The parameters n , d_1 , and d_2 are the same as those used in (d).

width of this narrow passband is related to the relative lengths of the two segments, and it can be obtained from the dispersion relation (13). If we denote $d_2 = (2 + \delta d)d_1$, where δd is a small number comparing to unity, then the width $\Delta\omega_{nar}$ of the narrow band is approximately

$$\Delta\omega_{nar} \approx \frac{\pi c}{2d_1} \delta d. \quad (16)$$

A finite-size SMCN can be studied by injecting waves into the node located at the center of the sample where all boundary nodes are connected to leads, from which the waves can leak out.¹¹ The waves in a finite-size SMCN with this kind of boundary condition will behave similarly to those in an infinite SMCN, since the waves in both situations are not confined. In our study, we inject a wave with unit amplitude into the sample for simplicity. The wave function at each node can be calculated by the generalized eigenfunction method,¹⁹ which was first introduced in studying the electronic transport properties.

The real part of the wave function at the frequency of approximately $\omega = 1.77(\pi c/d_1)$ for a sample with a size of 21×21 nodes and with $n=2$ and $d_2=2d_1$ is shown in Fig. 4, from which one can see that a Bloch mode is periodic with respect to the radial direction. Two real solutions of Eq. (13) for this frequency are approximately $\mathbf{K} = (0.5\pi, 0)$ and $(0.33\pi, 0.33\pi)$. Hence the propagating Bloch wave is required to be periodic with four discrete configuration translations along \mathbf{e}_1 and six along $\mathbf{e}_{1,2} = \mathbf{e}_1 + \mathbf{e}_2$, which is still approximately satisfied in the finite-size sample that all the boundary nodes are connected by leads.

We also plot the total transmission spectra of a finite-size SMCN in Fig. 3(e) for $n=2$ and $d_2=1.98d_1$, the same parameters used in Fig. 3(d). The total transmission spectra are calculated by summing over all the transmission coefficients at the boundary leads.¹¹ The comparison of Figs. 3(d) and 3(e) shows that the calculated band structure is consistent with the transmission spectra. The solid curve and the dashed curve plotted in Fig. 3(e) are the total transmission spectra of

the samples with a size of 10×10 and 15×15 nodes, respectively. The narrow peak in the vicinity of $\omega = \pi c/d_1$ arises from the transmission of propagation waves, and hence the amplitude will not decrease exponentially with the sample size. The large dips in the spectrum indicate that the attenuation in the band gaps is very strong. Notice that the largest attenuation is near the upper edge of the narrow passband. We will give more discussion on this feature later.

If we introduce a defect in a SMCN with parameters $n=2$ and $d_2=2d_1$ by changing the length of one segment at the center of the sample from $2d_1$ to $2.2d_1$, a defect state will be created. From the calculation of transmission spectra we found that the defect state locates at the frequency of approximately $1.43\pi c/d_1$. The corresponding intensity map $|\psi(\mathbf{N})|^2$ is shown in Fig. 5, from which a sharply localized state at the defect nodes is clearly seen (notice the two dark squares).

When the frequencies are inside a PBG, \mathbf{K} is complex with an imaginary part $\text{Im } \mathbf{K} = (\text{Im } K_1, \text{Im } K_2)$. The factor $e^{-2 \text{Im } K_1}$, which measures the attenuation of the wave intensity along \mathbf{e}_1 , for a SMCN with $n=3$ and $d_3=d_2=2d_1$ for different evanescent modes, is plotted in Fig. 6(b), including $K_1=K_2$ (circles), $K_2=0$ (crosses), and $K_2=\pi$ (triangles). We

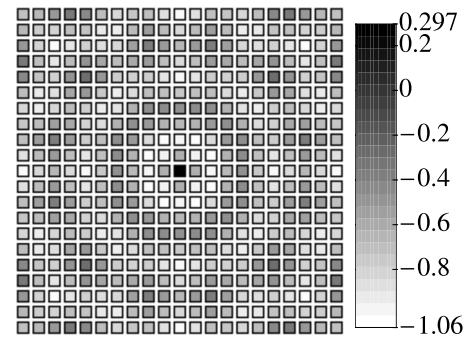


FIG. 4. Intensity map for the real part of ψ at the nodes of a SMCN with a size of 21×21 nodes and with parameters $n=2$ and $d_2=2d_1$. The frequency is approximately $\omega = 1.77\pi c/d_1$.

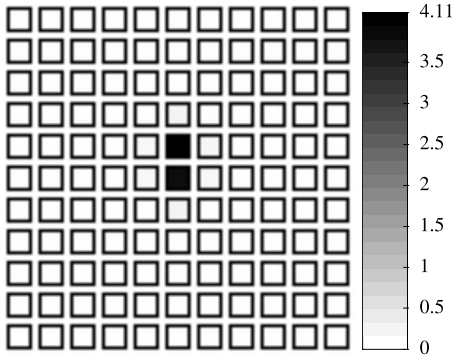


FIG. 5. Intensity map $|\psi|^2$ of a defect state at approximately $\omega = 1.43\pi c/d_1$. The two darkest squares correspond to the nodes between which a defect segment was introduced. The sample size is 11×11 nodes.

also calculated the total transmission coefficient $T_{11 \times 11}$ for a finite-size SMCN with 11×11 nodes and $T_{9 \times 9}$ with 9×9 nodes. The average attenuation per configuration translation for waves with frequencies in the band gap traveling in all directions can be obtained approximately by $T_{11 \times 11}/T_{9 \times 9}$, which is plotted by the solid curve in Fig. 6(b). One can see that this solid curve in the band gaps is between maximum and minimum of $e^{-2 \text{Im} K_1}$ for different modes. So the analytical attenuation calculation for different EM modes is consistent with the transmission calculation. The solid curve is closer to the larger $e^{-2 \text{Im} K_1}$, since the corresponding modes with less energy attenuation give a dominant contribution to the transmission spectrum.

As can be seen from Fig. 6(b), the attenuation for waves with frequency within the second gap is extremely large. Even for only one configuration translation, the EM waves are attenuated at least 40 dB at the frequency range from $0.886\pi c/d_1$ to $1.114\pi c/d_1$. The factor $e^{-2 \text{Im} K_1}$ approaches zero rapidly when the frequencies get closer to $\pi c/d_1$. For the first and third gaps, the attenuation is relatively small

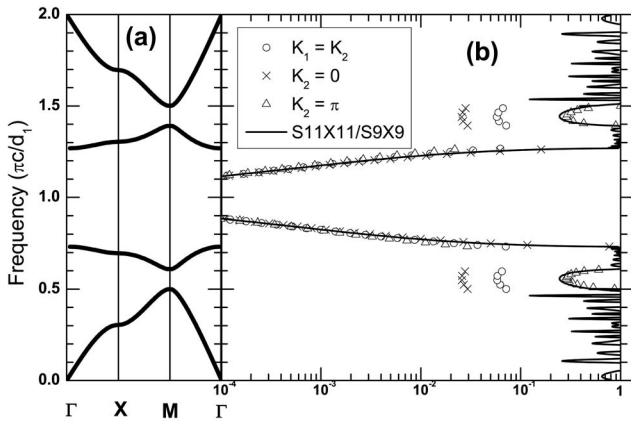


FIG. 6. (a) Band structure for a SMCN with $n=3$ and $d_3=d_2=2d_1$. (b) The attenuation per configuration translation. Circles, crosses, and triangles show the $e^{-2 \text{Im} K_1}$ for different attenuation modes with $K_1=K_2$, $K_2=0$, and $K_2=\pi$, respectively. The solid curve is $T_{11 \times 11}/T_{9 \times 9}$, the ratio of the total transmissions of two SMCNs for 11×11 and 9×9 nodes.

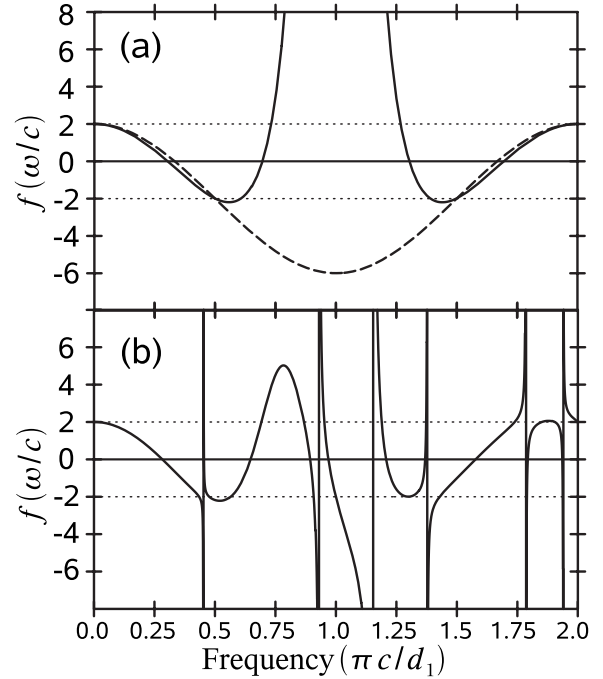


FIG. 7. (a) Solid curve is the plot of $f(\omega/c)$ for $n=3$ and $d_3 = d_2 = 2d_1$. Dashed curve is the case of $n=2$ and $d_2 = 2d_1$. (b) $f(\omega/c)$ with parameters $n=3$ and $d_3 = 2.05d_1$ and $d_2 = 2.15d_1$.

compared with that in the second gap; however, $e^{-2 \text{Im} K_1}$ can still be smaller than 0.1 for certain modes. Note that the attenuation for the $K_2=0$ mode is larger than that one with $K_2=\pi$ in the first and third gaps, whereas in the second gap the attenuation for the $K_2=\pi$ mode is stronger.

For clarity, we plot the function $f(\omega/c)$ in Eq. (13) in Fig. 7(a) by a solid curve for $n=3$ and $d_3=d_2=2d_1$. From the figure one can see that $f(\omega/c)$ is slightly smaller than -2 in the first and third gaps, while in the second gap it is much larger than 2 and approaches infinity when the frequencies get closer to $\pi c/d_1$, which is quite different from the case with frequencies within the first and second gaps. We also show $f(\omega/c)$ with parameters used in Fig. 3(a) in Fig. 7(a) by a dashed curve. It can be seen that even though the width of the large gap shown in Fig. 3(a) is larger than that of the second gap in Fig. 6(a), the attenuation in the former is smaller. This difference is due to the occurrence of strong resonance at resonance frequencies for which $f(\omega/c)$ approaches infinity.

If we change the ratios of the lengths of the three segments connecting the same nodes being not integers, $d_3 = 2.05d_1$ and $d_2 = 2.15d_1$, then $f(\omega/c)$ changes and more gaps and several narrow passbands are created, which can be seen from Fig. 7(b). Actually, the existence of an extremely narrow passband, such as the narrow band shown in Fig. 3(d), is a consequence of the strong resonance and antiresonance. At frequencies where there is an antiresonance, which inhibits forming a gap, $|f(\omega/c)|$ is required to be smaller than 2. If in the vicinity of these frequencies a strong resonance occurs, $f(\omega/c)$ tends towards infinity, and its slope will be very large; consequently a narrow passband is created near a gap with large attenuation.

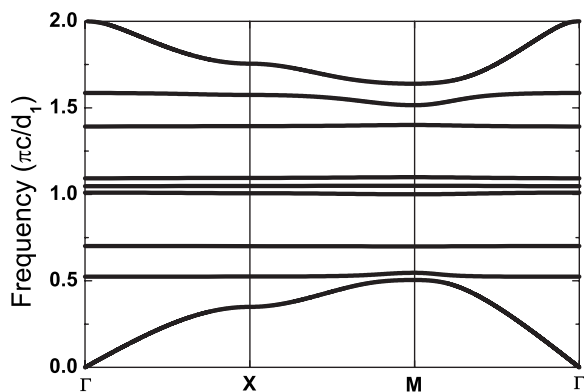


FIG. 8. Band structure for a SMCN. The parameters $n=4$ and $d_4:d_3:d_2:d_1=1.98:1.83:0.91:1$ are used.

For conventional PBG structure $\text{Im } \mathbf{K}$ has a quasiparabolic profile as a function of wave frequency inside a band gap.^{7,20} However, in SMCNs, $\text{Im } \mathbf{K}$ can reach infinity and its maximum may not locate at the center of the gap. These differences are due to the strong resonance and antiresonance in the segments connecting the same nodes.

If the number n of segments connecting every pair of nearest-neighbor nodes increases, more resonance modes will appear. As an example, we show the band structure for a SMCN with $n=4$ and $d_4:d_3:d_2:d_1=1.98:1.83:0.91:1$ in Fig. 8, from which one can see that more gaps are created and three narrow passbands appear in the vicinity of $\pi c/d_1$.

IV. CONCLUSIONS

We have shown that if the conventional Floquet-Bloch theorem is modified to be dimensionless, then it can still work in configuration-periodic networks, such as the SMCNs studied in this paper, in which the space translation symmetry may not hold and the period of the systems cannot be defined.

Due to the resonance and antiresonance behavior arising in the segments between nearest-neighbor nodes, wide gaps and narrow passbands are created. The phase \mathbf{K} , corresponding to the conventional Bloch wave vector, is complex in a band gap. Its imaginary part $\text{Im } \mathbf{K}$ describes the attenuation of a wave inside a PBG. We found that $\text{Im } \mathbf{K}$ has a unconventional profile as a function of wave frequency inside a band gap which results from a strong resonance and antiresonance. $\text{Im } \mathbf{K}$ (and hence the attenuation) can be very large in a system with appropriate parameters and approaches infinity at the resonance frequencies, which, however, may not be the midgap frequencies of the gaps. Since the attenuation is very large in the PBG, then the corresponding localization length is small; consequently, waves can be strongly confined in the defects. The attenuation constants are different for different \mathbf{K} values, even though the evanescent modes are of the same frequency and decay in the same direction.

The propagation properties of a SMCN can be tunable if the waveguide segments of different lengths are made of different materials. For example, changing temperature will alter the relative lengths of the segments. Therefore the band structures and the attenuation of waves can be tuned by temperature. The SMCNs with controllable gaps and passbands have potential applications.

Recently, coaxial photonic crystals (i.e., 1D networks made of alternating segments of two different types of ordinary coaxial cable) have been used to study the effects observed in conventional photonic crystals, including defect modes, superluminal wave-packet tunneling, and slow EM propagation.²¹⁻²³ It can be expected that SMCNs consisting of coaxial cables can be also used to study these effects in 2D and 3D.

ACKNOWLEDGMENTS

This work was supported by the National Natural Science Foundation of China, Grant No. 10004003, and the Program for Innovative Research Team of the Higher Education in Guangdong, Grant No. 06CXTD005.

*zhenyu3cn@gmail.com

†xbyang@scnu.edu.cn

¹E. Yablonovitch, Phys. Rev. Lett. **58**, 2059 (1987).

²S. John, Phys. Rev. Lett. **58**, 2486 (1987).

³Kerry J. Vahala, Nature (London) **424**, 839 (2003).

⁴P. Lodahl, A. Floris van Driel, I. S. Nikolaev, A. Irman, K. Overgaag, D. Vanmaekelbergh, and W. L. Vos, Nature (London) **430**, 654 (2004).

⁵S. W. Leonard, H. M. van Driel, K. Busch, S. John, A. Birner, A.-P. Li, F. Müller, U. Gösele, and V. Lehmann, Appl. Phys. Lett. **75**, 3063 (1999).

⁶Y. Neve-Oz, M. Golosovsky, D. Davidov, and A. Frenkel, J. Appl. Phys. **95**, 5989 (2004).

⁷C. Ciminelli, F. Peluso, and M. N. Armenise, Opt. Express **13**, 9729 (2005).

⁸Z. Q. Zhang, C. C. Wong, K. K. Fung, Y. L. Ho, W. L. Chan, S.

C. Kan, T. L. Chan, and N. Cheung, Phys. Rev. Lett. **81**, 5540 (1998).

⁹L. Dobrzynski, A. Akjouj, B. Djafari-Rouhani, J. O. Vasseur, and J. Zemmouri, Phys. Rev. B **57**, R9388 (1998).

¹⁰Z. Q. Zhang and P. Sheng, Phys. Rev. B **49**, 83 (1994).

¹¹S. K. Cheung, T. L. Chan, Z. Q. Zhang, and C. T. Chan, Phys. Rev. B **70**, 125104 (2004).

¹²I. V. Shadrivov, A. A. Sukhorukov, and Y. S. Kivshar, Phys. Rev. Lett. **95**, 193903 (2005).

¹³K. Samokhvalova, C. Chen, and B. L. Qian, J. Appl. Phys. **99**, 063104 (2006).

¹⁴M. Golosovsky, Y. Neve-Oz, D. Davidov, and A. Frenkel, Phys. Rev. B **70**, 115105 (2004).

¹⁵J. Huang, N. Eradat, M. E. Raikh, Z. V. Vardeny, A. A. Zakhidov, and R. H. Baughman, Phys. Rev. Lett. **86**, 4815 (2001).

¹⁶A. Mir, A. Akjouj, J. O. Vasseur, B. Djafari-Rouhani, N. Fettouhi,

- E. H. El Boudouti, L. Dobrzynski, and J. Zemmouri, *J. Phys.: Condens. Matter* **15**, 1593 (2003).
- ¹⁷L. Dobrzynski, *Surf. Sci.* **180**, 489 (1987).
- ¹⁸W. M. Robertson, J. Pappafotis, P. Flannigan, J. Cathey, B. Cathey, and C. Klaus, *Appl. Phys. Lett.* **90**, 014102 (2007).
- ¹⁹Y. Liu, Z. Hou, P. M. Hui, and W. Sritrakool, *Phys. Rev. B* **60**, 13444 (1999).
- ²⁰E. Istrate, A. A. Green, and E. H. Sargent, *Phys. Rev. B* **71**, 195122 (2005).
- ²¹G. J. Schneider, S. Hanna, J. L. Davis, and G. H. Watson, *J. Appl. Phys.* **90**, 2642 (2001).
- ²²J. N. Munday and W. M. Robertson, *Appl. Phys. Lett.* **83**, 1053 (2003).
- ²³A. Haché and S. Essiambre, *Phys. Rev. E* **69**, 056602 (2004).